



Giant Nonlocality Near the Dirac Point in Graphene

D. A. Abanin, et al. Science **332**, 328 (2011); DOI: 10.1126/science.1199595

This copy is for your personal, non-commercial use only.

If you wish to distribute this article to others, you can order high-quality copies for your colleagues, clients, or customers by clicking here.

Permission to republish or repurpose articles or portions of articles can be obtained by following the guidelines here.

The following resources related to this article are available online at www.sciencemag.org (this infomation is current as of April 14, 2011):

Updated information and services, including high-resolution figures, can be found in the online version of this article at:

http://www.sciencemag.org/content/332/6027/328.full.html

Supporting Online Material can be found at:

http://www.sciencemag.org/content/suppl/2011/04/13/332.6027.328.DC1.html

This article **cites 22 articles**, 1 of which can be accessed free: http://www.sciencemag.org/content/332/6027/328.full.html#ref-list-1

This article has been **cited by** 1 articles hosted by HighWire Press; see: http://www.sciencemag.org/content/332/6027/328.full.html#related-urls

This article appears in the following **subject collections**: Physics

http://www.sciencemag.org/cgi/collection/physics

Giant Nonlocality Near the Dirac Point in Graphene

D. A. Abanin, ^{1,2} S. V. Morozov, ^{1,6} L. A. Ponomarenko, ¹ R. V. Gorbachev, ¹ A. S. Mayorov, ¹ M. I. Katsnelson, ³ K. Watanabe, ⁴ T. Taniguchi, ⁴ K. S. Novoselov, ¹ L. S. Levitov, ⁵* A. K. Geim¹*

Transport measurements have been a powerful tool for discovering electronic phenomena in graphene. We report nonlocal measurements performed in the Hall bar geometry with voltage probes far away from the classical path of charge flow. We observed a large nonlocal response near the Dirac point in fields as low as 0.1 tesla, which persisted up to room temperature. The nonlocality is consistent with the long-range flavor currents induced by the lifting of spin/valley degeneracy. The effect is expected to contribute strongly to all magnetotransport phenomena near the neutrality point.

raphene continues to attract intense in--terest, especially as an electronic system in which charge carriers are Dirac-like particles with linear dispersion and zero rest mass. Transport measurements in graphene have unveiled a number of unusual phenomena, including two new types of the quantum Hall effect (QHE), minimum metallic conductivity, bipolar superconductivity, and Klein scattering (1-4). In a number of experiments, unusual behavior was found at low temperatures (T) and high magnetic fields (B) near the so-called Dirac or neutrality point (NP), where charge carrier density n tends to zero (5-9). However, the NP is also hardest to access experimentally because of charge inhomogeneity (electron-hole puddles) and limited carrier mobilities (u). Furthermore, the fundamental neutral degrees of freedom in graphene, such as spin and valley, evade detection by the standard electrical measurement techniques, even in the best-quality samples (here the valley degree of freedom refers to the inequivalence of the pair of conical valence/conduction bands in the Brillouin zone, which touch at Dirac points).

In this work, we performed nonlocal measurements, previously used to probe the dynamics of population imbalance for edge modes in quantum Hall systems (10, 11) as well as spin diffusion (12) and magnetization dynamics (13). The advantage of nonlocal measurements is that they allow one to filter out the ohmic contribution resulting from charge flow and, in doing so, detect more subtle effects that otherwise can remain unnoticed (10-14). The measurements

¹Manchester Centre for Mesoscience and Nanotechnology, University of Manchester, Manchester M13 9PL, UK. ²Princeton Center for Theoretical Science and Department of Physics, Princeton University, Princeton, NJ 08544, USA. ³Theory of Condensed Matter, Institute for Molecules and Materials, Radboud University Nijmegen, Heyendaalseweg 135, 6525 AJ Nijmegen, Netherlands. ⁴National Institute for Materials Science, 1-1 Namiki, Tsukuba, 305-0044 Japan. ⁵Department of Physics, Massachusetts Institute of Technology, Cambridge, MA 02139, USA. ⁶Institute for Microelectronics Technology, 142432 Chernogolovka, Russia.

*To whom correspondence should be addressed. E-mail: levitov@mit.edu (L.S.L.); geim@man.ac.uk (A.K.G.)

were carried out by using more than 20 devices of two different types. Type I devices were made in the conventional way, with graphene placed on top of an oxidized Si wafer (1-7), hereafter referred to as GSiO. Type II devices contained thin crystals of hexagonal boron nitride placed between graphene and SiO₂ (15) (referred to as GBN). All the devices were made in the Hall bar geometry by following the microfabrication procedures described previously (1, 6, 15–17). The GSiO devices had mobility μ of ~10,000 cm²/Vs, whereas GBN devices showed much higher μ , between 50,000 and 150,000 cm²/Vs for carrier concentrations $n \sim 10^{11} \text{ cm}^{-2}$ (17). Typical charge inhomogeneity n_0 estimated from the rounding of the conductivity minimum was $\sim 10^{10}$ and 10^{11} cm⁻² for GBN and GSiO devices, respectively. All of our samples exhibited a qualitatively similar nonlocal response; however, its absolute value was 10 to 100 times larger in GBN samples. Unless stated explicitly, the results described below refer equally to both device types.

Figure 1A shows a representative GSiO device, used to describe different measurement geometries. In the standard Hall bar geometry, so that current I_{14} flows between contacts 1 and 4 and voltage V_{23} is measured between contacts 2 and 3, the longitudinal resistivity ρ_{xx} [calculated as $(w/L) \times R_{23,14}$, where L and w are the length and width of the Hall bar, and $R_{23,14} = V_{23}/I_{14}$] shows the standard QHE behavior for monolayer graphene, with wide regions of zero ρ_{xx} accompanied by well-defined plateaus in Hall resistivity ρ_{xy} (Fig. 1B and fig. S1).

In the following, we focus on the nonlocal resistance, $R_{\rm NL}$. The measured signal (e.g., $R_{35,26}$ in Fig. 1C) cannot be understood in terms of the classical picture of charge flow. Indeed, a fraction of applied current I_{26} , which flows sideways and reaches the remote region between contacts 3 and 5, is exponentially small in the separation L. Using the van der Pauw formalism (18), it is straightforward to show that the expected Ohm's law contribution to $R_{\rm NL}$ behaves as $\approx \rho_{xx} \exp(-\pi L/w)$ for both zero and nonzero B (17). For our devices, L ranged from 3 to 15 μm and w between 1 and 2 μ m. For a typical L/w = 5, this translates into minute $R_{\rm NL} < 10^{-3}$ ohm. In agreement with this estimate, $R_{NL}(B = 0)$ was indistinguishable from zero at our maximum resolution (Fig. 1C).

The situation changes radically in finite B: $R_{\rm NL}$ remains zero at zeros of ρ_{xx} , but between the QHE zeros it can reach values of ~1 kilohm, even in the conventional GSiO devices, and exhibits the same overall oscillating pattern as ρ_{xx} (Fig. 1C). Although the pattern always remained the same, the amplitude of the nonlocal response varied significantly for different devices. In particular, $R_{\rm NL}$ depended on an exact contact configuration (that is, $R_{35,26} \neq R_{34,26}$), yet with the Onsager relation $R_{35,26}(B) \neq R_{26,35}(B) = R_{35,26}(-B)$ satisfied (fig. S3). $R_{\rm NL}$ was found to become smaller with increasing L and in the presence of

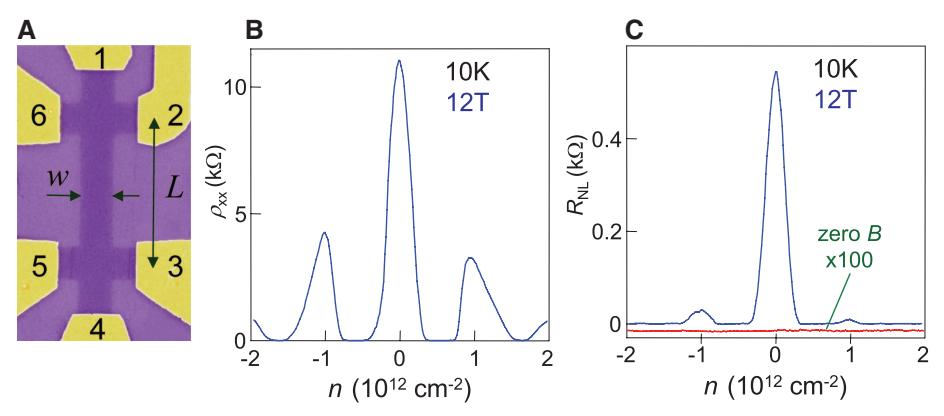


Fig. 1. Local and nonlocal geometries. **(A)** Electron micrograph (false color) of a GSiO device. The width $w = 1 \mu m$ and length L of the Hall bar are indicated. **(B)** Longitudinal resistivity ρ_{xx} as a function of carrier density n in a perpendicular B = 12 T. **(C)** In the nonlocal geometry, no signal can be detected in zero B (the red curve is downshifted for clarity and magnified). The magnetic field gives rise to large R_{NL} shown for standard-quality devices (GSiO type). To ensure that there was no contribution from inductive coupling and thermopower, we used both dc and low-frequency ac measurements with typical driving currents I of $1 \mu A$. R_{NL} was confirmed to be independent of I by varying it over two orders of magnitude.

extra leads between current and voltage contacts (fig. S3). The strong sample and contact dependence did not allow us to quantify the spatial scale involved in the nonlocality, but it can be estimated as exceeding L (that is, $\sim 10 \, \mu m$) in $B > 5 \, \mathrm{T}$ and $T < 100 \, \mathrm{K}$. To emphasize the importance of nonlocal transport near the NP, in (17) we describe the standard Hall measurements in two configurations, $R_{35,42}$ and $R_{35,46}$, where the same voltage probes were used and the only difference was the swap of one of the current leads. In a classical conductor, this should cause no effect whatsoever, but in graphene, nonlocal transport leads to profound differences between the two supposedly equivalent measurements (fig. S1).

To elucidate the origin of the unexpected nonlocality at the NP, we studied its T and B dependence. The peaks in $R_{\rm NL}$ at filling factors v = 4 and 8 completely disappear above 70 K, simultaneously with the disappearance of the zeros in $\rho_{\rm xx}$. Therefore, the nonlocality at v = 4 and 8 can be attributed to the standard QHE edge-state transport (10, 11). In contrast, the nonlocal signal at the NP (v = 0) is found to be much more robust (Fig. 2), extending well beyond the QHE regime, into the regime where even Shubnikov–de Haas

oscillations are completely absent. At 300 K, the nonlocality remains quite profound, with $R_{\rm NL} \sim 1$ kilohm at several tesla and a remnant signal observable in B << 1 T. This behavior implies that the nonlocality at the NP occurs via a mechanism that is different from the QHE edge-state transport (10, 11, 17).

Figure 2C reveals two temperature regimes. At high T, R_{NL} decreases slowly with increasing T, whereas below ~30 K, one can see a rapid increase in $R_{\rm NL}$. The latter correlates with an increase in ρ_{xx} for GBN devices and can be attributed to the onset of an energy gap that opens at v = 0 at low T(5, 7, 9, 15). By using the Corbino geometry, we found that the gap did not exceed 20 K at 12 T for GSiO (17). Similar values were reported by other groups (7, 19). For certain gapped states, the nonlocality can arise because of countercirculating edge states (6). To test this possibility, we carried out nonlocal measurements on devices patterned to have a channel widening that increased devices' edge length more than 10-fold, while L between the current and voltage contacts remained the same (17). No significant difference in $R_{\rm NL}$ was observed in such devices as compared to those with no widening.

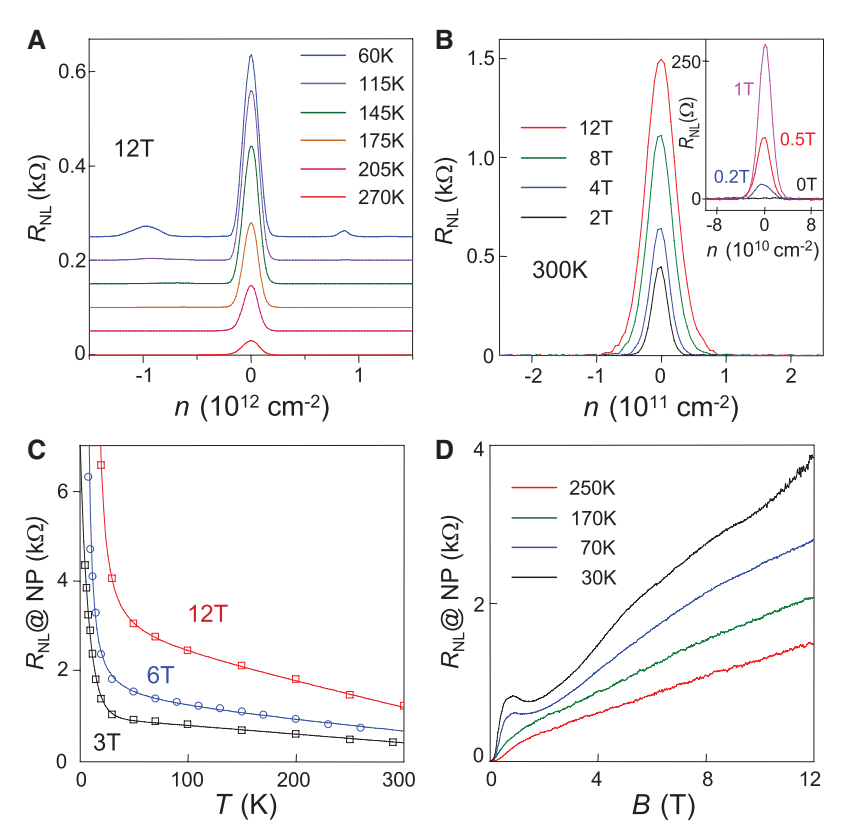


Fig. 2. Nonlocal transport in graphene. (**A**) $R_{\rm NL}$ for the GSiO device in Fig. 1 at different T. In high B, the nonlocality at v=4 persists up to liquid nitrogen T. The nonlocal signal at the NP is even more robust with increasing T. (**B**) Room-T $R_{\rm NL}$ for a GBN device with $\mu\approx 140,000~{\rm cm^2/Vs}$, and with nonlocal voltage contacts separated from the current path by $L=5~{\rm \mu m}$. The inset magnifies $R_{\rm NL}$ in small B. Even at 0.1 T, $R_{\rm NL}$ remains substantial (~10 ohm). GSiO devices exhibit a qualitatively similar behavior but with room-T values of $T_{\rm NL}$ and $T_{\rm NL}$ at the NP as a function of $T_{\rm NL}$ for several values of $T_{\rm NL}$ and as a function of $T_{\rm NL}$ for several values of $T_{\rm NL}$ at the NP as a function of $T_{\rm NL}$ for several values of $T_{\rm NL}$ and $T_{\rm NL}$ for several values of $T_{\rm NL}$ and $T_{\rm NL}$ for the same GBN device as in (B). The solid curves in (C) are quides to the eye.

This and other observations described in (17) provide evidence against edge transport and suggest a bulk transport mechanism even in the low-T gapped state. This conclusion is also consistent with the insulating behavior found in previous magnetotransport studies at the NP (5, 7, 9, 15). The observed sharp increase in $R_{\rm NL}$ at low T (Fig. 2C) may indicate that the dominant nonlocality mechanism changes as the system goes into the gapped state.

Below we discuss the high-T regime, where the gap opening at the NP is irrelevant, because no nonlocal signal could be detected even at v = 4and 8, despite cyclotron gaps being large (~500 K). The nonlocality observed at high T and low Bcalls for a quasiclassical explanation that does not involve Landau quantization. At the same time, one has to find a mechanism that naturally extends into the low-T regime, where the observed nonlocality becomes increasingly more profound. One possible explanation is the flavor Hall effect (FHE), a bulk mechanism in which nonlocality is mediated by neutral excitations, such as spin and valley flavors, and which works in both quasiclassical and QHE regimes, providing a natural explanation for our experimental findings (17).

The basic physics of the FHE is illustrated in Fig. 3, which for simplicity refers to the case of spin. The Zeeman splitting shifts the Dirac cones for opposite spin projections relative to each other. At the NP, the spin splitting produces a finite concentration of electrons with spin-up (1) and holes with spin-down (1) (Fig. 3A). When electric current is applied, the Lorentz force creates opposite spin-up and spin-down currents, leading to a spatial spin imbalance at zero net Hall voltage at the NP (Fig. 3B). The phenomenology is similar to the spin Hall effect (SHE) resulting from spin-orbit interaction (20–22), yet our SHE effect relies on the Zeeman splitting induced by B and occurs in the absence of spin-orbit interaction. In graphene, the SHE can generate long-range spin currents, due to slow spin relaxation (2, 23), and produce a nonlocal voltage at a remote location via a reverse SHE, as illustrated in Fig. 3B.

Figure 3C plots the modeled SHE behavior for $R_{\rm NL}$ in GSiO, which captures the main features of the experimental data, most importantly the peak at the NP in $R_{\rm NL}(n)$. The model also predicts maximum value $R_{\rm NL} \sim h/4e^2$, which corresponds to a cutoff due to Landau level broadening (17). Such values are indeed observed in GBN devices (Fig. 2C). The T and B dependences predicted from the simple model are in qualitative agreement with the experiment. The agreement can be further improved by taking into account valley splitting that can give rise to neutral valley currents and additional nonlocality. In particular, the onset of the valley splitting due to interaction effects (19) may be responsible for the observed increase in $R_{\rm NL}$ below 30 K. Although our measurements did not probe flavor currents directly, the indirect evidence is overwhelming. The nonlocal phenomena are very rare and, given that we have ruled out

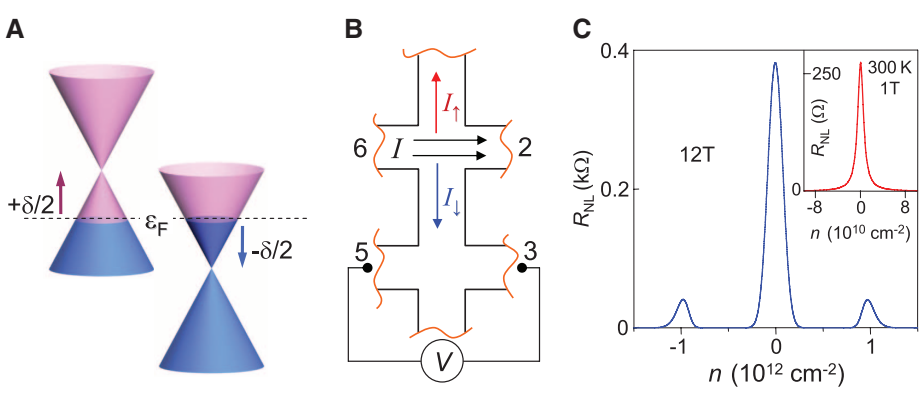


Fig. 3. SHE in graphene and nonlocal transport mediated by spin diffusion. **(A)** Zeeman splitting at charge neutrality produces two pockets filled with electrons and holes having opposite spin. **(B)** In the presence of the Lorentz force, *I* gives rise to transverse spin currents I_{\uparrow} and I_{\downarrow} . Because the force has opposite signs for electrons and holes, the net charge current is zero, whereas the net spin current is nonzero. The resulting imbalance in the up/down spin distribution can reach remote regions and generate a voltage drop *V*. **(C)** $R_{\rm NL}$ predicted in our model for the QHE regime (main panel) and the quasiclassical regime (inset). The best-fit parameters $n_0 = 4 \times 10^9$ cm⁻² and Landau level broadening $\Gamma = 200$ K are typical for GBN and GSiO devices, respectively. $R_{\rm NL}$ grows with decreasing n_0 and Γ (17), which is consistent with much larger $R_{\rm NL}$ measured in our GBN devices.

edge-state transport mechanisms, we believe that the spin/valley Hall effect is the only remaining explanation for our findings.

The profound nonlocality described here is an essential attribute of electron transport in graphene. The nonlocality is consistent with neutral currents generated by the SHE at high *T* and, possibly, by the valley Hall effect at liquid-helium *T*. Nonlocal transport, being directly sensitive to neutral degrees of freedom, provides valuable in-

formation that is inaccessible by conventional electrical measurements.

References and Notes

- 1. A. K. Geim, K. S. Novoselov, *Nat. Mater.* **6**, 183 (2007).
- A. H. Castro Neto, F. Guinea, N. M. R. Peres,
 K. S. Novoselov, A. K. Geim, *Rev. Mod. Phys.* 81, 109 (2009)
- 3. H. B. Heersche, P. Jarillo-Herrero, J. B. Oostinga, L. M. Vandersypen, A. F. Morpurgo, *Nature* **446**, 56

- 4. A. F. Young, P. Kim, Nat. Phys. 5, 222 (2009).
- J. G. Checkelsky, L. Li, N. P. Ong, Phys. Rev. B 79, 115434 (2009).
- 6. D. A. Abanin *et al.*, *Phys. Rev. Lett.* **98**, 196806 (2007).
- Z. Jiang, Y. Zhang, H. L. Stormer, P. Kim, *Phys. Rev. Lett.* 99, 106802 (2007).
- 8. B. E. Feldman, J. Martin, A. Yacoby, *Nat. Phys.* **5**, 889 (2009).
- X. Du, I. Skachko, F. Duerr, A. Luican, E. Y. Andrei, Nature 462, 192 (2009).
- 10. P. L. McEuen et al., Phys. Rev. Lett. 64, 2062 (1990).
- 11. R. J. Haug, Sem. Sci. Tech. 8, 131 (1993).
- Y. Tserkovnyak, S. Brataas, G. E. W. Bauer, B. I. Halperin, Rev. Mod. Phys. 77, 1375 (2005).
- F. J. Jedema, M. S. Nijboer, A. T. Filip, B. J. van Wees, *Phys. Rev. B* 67, 085319 (2003).
- 14. S. Washburn, R. A. Webb, Rep. Prog. Phys. 55, 1311 (1992).
- 15. C. R. Dean et al., Nat. Nanotechnol. 5, 722 (2010).
- 16. R. V. Gorbachev et al., Small 7, 465 (2011).
- 17. See supporting material on Science Online.
- 18. L. J. van der Pauw, Philips Tech. Rev. 20, 220 (1958).
- 19. Y. J. Song et al., Nature 467, 185 (2010).
- 20. J. Sinova et al., Phys. Rev. Lett. 92, 126603 (2004).
- Y. K. Kato, R. C. Myers, A. C. Gossard, D. D. Awschalom, Science 306, 1910 (2004).
- J. Wunderlich, B. Kaestner, J. Sinova, T. Jungwirth, *Phys. Rev. Lett.* 94, 047204 (2005).
- N. Tombros, C. Jozsa, M. Popinciuc, H. T. Jonkman,
 B. J. van Wees, *Nature* 448, 571 (2007).
- 24. Supported by the Engineering and Physical Research Council (UK), the Royal Society, U.S. Office of Naval Research, U.S. Air Force Office of Scientific Research, and the Körber Foundation. We thank D. Elias, P. Blake, E. Hill, F. Schedin, S. Anissimova, and I. Grigorieva for their help.

Supporting Online Material

www.sciencemag.org/cgi/content/full/332/6027/328/DC1 SOM Text Figs. S1 to S8

Figs. S1 to S8 References

26 October 2010; accepted 28 February 2011 10.1126/science.1199595

Teleportation of Nonclassical Wave Packets of Light

Noriyuki Lee,¹ Hugo Benichi,¹ Yuishi Takeno,¹ Shuntaro Takeda,¹ James Webb,² Elanor Huntington,² Akira Furusawa¹*

We report on the experimental quantum teleportation of strongly nonclassical wave packets of light. To perform this full quantum operation while preserving and retrieving the fragile nonclassicality of the input state, we have developed a broadband, zero-dispersion teleportation apparatus that works in conjunction with time-resolved state preparation equipment. Our approach brings within experimental reach a whole new set of hybrid protocols involving discrete- and continuous-variable techniques in quantum information processing for optical sciences.

In the early development of quantum information processing (QIP), a communication protocol called quantum teleportation was discovered (1) that involves the transportation of an unknown arbitrary quantum state $|\psi\rangle$ by means of entanglement and classical information. Ex-

¹Department of Applied Physics, School of Engineering, University of Tokyo, 7-3-1 Hongo, Bunkyo-ku, Tokyo 113-8656, Japan. ²Centre for Quantum Computation and Communication Technology, School of Engineering and Information Technology, University College, University of New South Wales, Canberra, ACT 2600, Australia.

*To whom correspondence should be addressed. E-mail: akiraf@ap.t.u-tokyo.ac.jp

perimental realizations of quantum teleportation (2, 3) and more advanced related operations (4) in the continuous-variable regime have been achieved by linear optics methods, although only for Gaussian states so far. However, at least third-order nonlinear operations are necessary for building a universal quantum computer (5)—something that Gaussian operations and Gaussian states alone cannot achieve. Photon subtraction techniques based on discrete-variable technology can provide useful nonlinearities and are used to generate Schrödinger's-cat states and other optical non-Gaussian states (6). Schrödinger's-cat states are of particular interest in this context, as they

have been shown to be a useful resource for faulttolerant QIP (7). It is therefore necessary to extend the continuous-variable technology to the technology used in the world of non-Gaussian states.

We have combined these two sets of technologies, and here we demonstrate such Gaussian operations on nonclassical non-Gaussian states by achieving experimental quantum teleportation of Schrödinger's-cat states of light. Using the photon subtraction protocol, we generate quantum states closely approximating Schrödinger's-cat states in a manner similar to (8-11). To accommodate the required time-resolving photon detection techniques and handle the wave-packet nature of these optical Schrödinger's-cat states, we have developed a hybrid teleporter built with continuous-wave light yet able to directly operate in the time domain. For this purpose we constructed a time-gated source of Einstein-Podolsky-Rosen (EPR) correlations as well as a classical channel with zero phase dispersion (12). We were able to bring all the experimental parameters up to the quantum regime, and we performed successful quantum teleportation in the sense that both our input and output states are strongly nonclassical.

A superposition of the quasi-classical coherent state $|\alpha\rangle$ is one of the consensus definitions of a Schrödinger's-cat state $|\text{cat}\rangle$, typically written